IEEE Open Journal of Ultrasonics, Ferroelectrics, and Frequency Control

Received 21 May 2022; revised 13 July 2022; accepted 1 August 2022.
Date of publication 5 August 2022; date of current version 22 August 2022.

*Digital Object Identifier 10.1109/OJUFFC.2022.3197126*

# Data-Over-Sound With PMUTs

**HARSHVARDHAN GUPTA [1,2] (Student Member, IEEE), BIBHAS NAYAK [1,3], ANUJ ASHOK [1,4] (Student Member, IEEE), AND RUDRA PRATAP [1,5] (Senior Member, IEEE)**

[1] Centre for Nano Science and Engineering, Indian Institute of Science, Bengaluru 560012, India
[2] Electrical and Computer Engineering (ECE), Carnegie Mellon University, Pittsburgh, PA 15213 USA
[3] Reliance Jio Tesseract Pvt. Ltd., Mumbai 400701, India
[4] Elmore Family School of Electrical and Computer Engineering, Purdue University, West Lafayette, IN 47907 USA
[5] Plaksha University, Sahibzada Ajit Singh Nagar 140306, India

CORRESPONDING AUTHOR: H. GUPTA (harshvardhan.gupta@gmail.com)

This work was supported in part by ToneTag, Naffa Innovations Pvt. Ltd.; and in part by the Nanoelectronics Network for Research and Applications (NNetRA).

**ABSTRACT** Data-over-sound is an emerging technology for digital communication which uses frequencies at the upper bounds of human hearing, usually between 15 kHz to 25 kHz. We report a successful development of Piezoelectric Micromachined Ultrasound Transducers (PMUTs) for low-power data-over-sound applications. Piezoelectric thin films used in PMUTs can have high residual tensile stresses ranging from 300 MPa to 1.5 GPa. These stresses have the effect of increasing the resonant frequencies of the transducers, making it a challenge to fabricate low frequency devices. Using the optimum dimensions by estimating the net residual stress in the fabricated diaphragms, transducers suitable for a frequency range of 17 kHz to 21 kHz were fabricated, capable of generating as much as 83 dB of sound pressure level at a distance of 5 cm in continuous operation.

**INDEX TERMS** PMUT, data-over-sound, aerial acoustic communication, PZT, thin-film stress, air-coupled, ultrasound.

## I. INTRODUCTION

DATA-OVER-SOUND (DoS), also known as Aerial Acoustic Communication (AAC) is a communication protocol [1] that utilizes signals at the upper bounds of human hearing (above 15 kHz). It is steadily gaining popularity in a number of industrial and consumer applications such as entry systems for public transport, contact-less transactions, inventory management, and proximity-based customer engagement — all using sound waves. This wireless communication protocol has its advantages over the widely used Bluetooth and Wi-Fi for localized data exchanges within a small physical distance. It has advantages in terms of secure and localized data exchanges when compared to radio waves, given that the acoustic waves (periodic pressure disturbances) with wavelengths near the ultrasonic range do not pass through barriers and are simply reflected off the walls of a typical room. Its hardware only requires a speaker and a microphone, which are present in audio-video equipment and every smartphone, and increasingly in wearables, smart appliances and IoT devices.

For DoS applications, the lower frequency limit is typically set above 18 kHz because the near-ultrasonic band of signals is difficult for most humans to perceive. The upper frequency limit for DoS is determined by the maximum sampling frequency, $f_s$, of recording systems in everyday appliances. For example, smartphones typically record their microphone signals at an $f_s$ of at least 44.1 kHz, which defines an upper working limit of around 22 kHz for DoS, according to the Nyquist-Shannon sampling theorem.

One of the main hardware concerns with DoS is that the majority of the available audio transducers are power hungry, which severely limits their applicability in cases where extended battery life is desired. Microspeakers, which are generally of the moving coil type, can draw large amounts of power when reproducing near ultrasonic frequencies at a suitable output acoustic pressure.

Piezoelectric micromachined ultrasonic transducers (PMUTs) have been a subject of research and development in MEMS for the past few decades. A PMUT is typically a multilayered MEMS structure that is fabricated by the deposition and patterning of its constituent piezoelectric and electrode films on a structural layer, followed by the release of this multistack diaphragm by backside etching. Their piezoelectric nature allows them to be used for both

This work is licensed under a Creative Commons Attribution 4.0 License. For more information, see https://creativecommons.org/licenses/by/4.0/

transmitting and receiving ultrasound. Operating frequencies for PMUTs generally range from a few tens of kHz to hundreds of MHz. With a small footprint and low power draw, they find use in applications such as non destructive evaluation [2], photoacoustic imaging [3], [4], fingerprint sensing [5], range finding [6] and density sensing [7].

However, fabricating PMUTs with low resonant frequencies has been a challenge due to the residual tensile stresses in their constituent layers that lead to fabricated devices exhibiting much higher resonant frequencies. In this paper, we describe a successful attempt at developing PMUTs with near-ultrasound resonant frequencies that suitably address the hardware concern for DoS. This was possible by estimating the value of the residual stress in the PMUT, modeling its influence on the natural frequency of the PMUT, and determining the optimal dimensions for a low resonant frequency. The preliminary results from this work were presented at the IUS 2020 [8]. This journal paper expands on the theory, design, and characterization of the transducers.

PZT (Lead Zirconate Titanate) is a piezoelectric material that is rather popular in PMUTs due to its high piezoelectric coefficients. PZT thin films are deposited either by physical methods such as sputtering or pulsed laser deposition, or by solution based methods such as the commonly used sol-gel process. Depending on the process and the deposition conditions, the magnitude of the residual stress can vary widely. The effects of stress on the performance of ultrasound transducers has been treated analytically by many previous authors [9], [10], [11], [12].

## II. STATE OF THE ART

PMUTs have been a subject of research and development since the 1990s. PMUTs with frequencies ranging from around 30 kHz to several GHz have been reported in the literature using a variety of piezoelectric and structural materials, and have been demonstrated as a viable replacement for conventional ultrasound transducers for various applications. High frequencies are preferred for imaging applications where they improve the resolution.

We limit our discussion to air-coupled applications, where PMUTs are mainly used for ranging and gesture recognition. Air-coupled ultrasound applications beyond 200 kHz are rare and limited to a few millimetres, since atmospheric sound absorption increases with frequency.

The specifications of a few air-coupled PMUTs found in the literature are listed in Table 1, arranged by ascending frequency. No studies were found on PMUTs with frequencies lower than 30 kHz.

Fabricating PMUTs with low frequencies is challenging due to several reasons:

1) Lower frequencies require large and thin diaphragms, that can be challenging to fabricate, handle, and package. PMUTs with diameters up to 1 mm had been fabricated in our lab before this study, with frequencies as low as 75 kHz [16]. Larger diaphragms are more delicate and can easily rupture after release.

**TABLE 1. Frequencies, piezoelectric materials used, and sizes for air-coupled PMUTs in the literature.**

| Authors | Frequency | Material | Size |
|---|---|---|---|
| P. Simeoni et al. [13] | 32 kHz | $LiNbO_3$ | 120 µm |
| Guo-Lun Luo et al. [14] | 40 kHz | PZT | 1250 µm |
| P. Simeoni and G. Piazza [15] | 45 kHz | AlN | 100 µm |
| A. Dangi and R. Pratap [16] | 75 kHz | PZT | 1000 µm |
| Zhihong Wang et al. [17] | 96 kHz | PZT | 1500 µm |
| K.H. Been et al. [18] | 100 kHz | PZT | 1500 µm |
| G. Massimino et al. [19] | 100 kHz | PZT | 880 µm |
| K. Roy et al. [7] | 140 kHz | PZT | 1000 µm |
| Zhen Zhou et al. [20] | 154 kHz | PMnN-PZT | 700 µm |
| Richard J. Przybyla et al. [21] | 214 kHz | AlN | 400 µm |

2) The presence of residual tensile stress in the PZT films increases the resonant frequency of the PMUTs. Similar to how tension in a drum skin increases its resonant frequency, residual stresses developed during fabrication processes increase the frequency of PMUTs. The effects of residual stress on ultrasound transducers have been studied analytically by Sammoura *et al.* [9] and Dangi and Pratap [10]. The parameters were simplified to non-dimensional quantities. Though this has given a good understanding of trends, actual design needs real numbers.
3) The presence of pin-hole and crack defects in PZT thin films can lead to electrical shorts between the top and the bottom electrode, leading to failure of the device. The probability of device failure due to defects increases with diaphragm size, and even a single defect over a large electrode area can render the transducer nonfunctional.

In this work, we push the limits of these transducers to fabricate devices with lower frequencies than ever reported in the literature. An analytical model is used to obtain design maps of pre-stressed PMUTs, which is subsequently verified with finite element simulations. The design maps are used to optimize the parameters of the PMUT to tune their frequencies and obtain devices with small footprints and high efficiencies.

The various design parameters of the transducers can be controlled to different degrees before, during and after fabrication. Before we delve into design optimization, we take a quick look at the microfabrication processes to understand how the dimensions of a PMUT are controlled and to what extent they can be varied.

## III. FABRICATION

The most common way to fabricate PMUTs is using a process involving highly anisotropic Deep Reactive Ion Etching (DRIE) of silicon to selectively etch the handle layer of a silicon-on-insulator (SOI) wafer and release the top layers to form the diaphragm. SOI wafers are used because they allow for the fabrication of diaphragms with very uniform

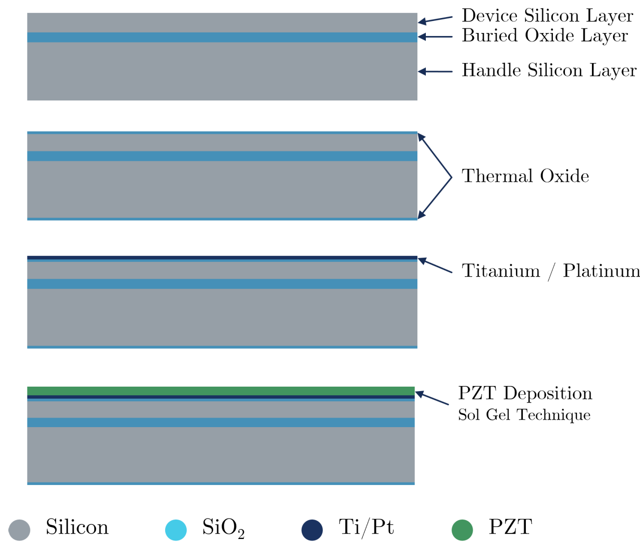


**FIGURE 1. Preparation of the SOI wafer—thermal oxidation, bottom electrode deposition and PZT deposition.**

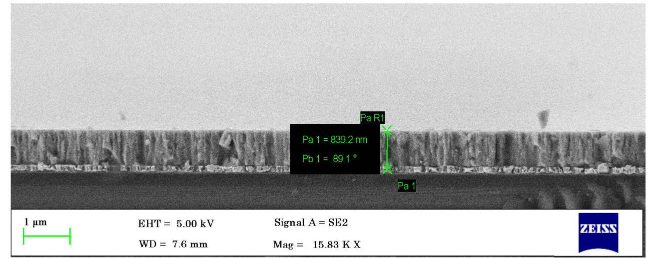


**FIGURE 2. Thin-film stack under SEM showing thickness of PZT deposited on platinum.**

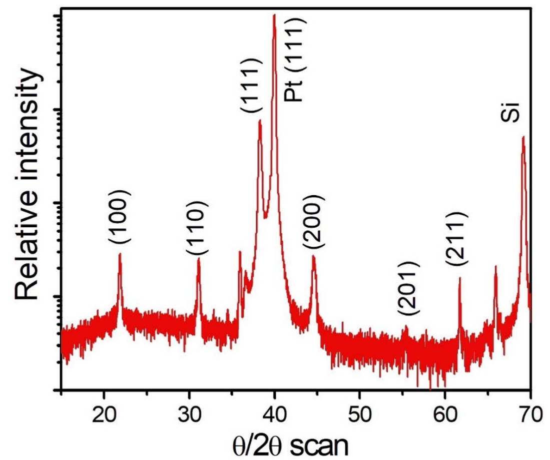


**FIGURE 3. X-ray diffraction (XRD) pattern of the Quintess PZT film.**

thickness even in the presence of process variations. The thickness of the passive structural layer in the PMUT diaphragm is determined by the thickness of the device layer of the SOI wafer.

Figure 1 shows a process flow of the wafer preparation for PMUTs. The process starts with a fresh SOI wafer that undergoes a dry or pyrogenic oxidation process to grow a silicon oxide layer on both sides of the wafer. The thickness of this thermally grown oxide is typically between 200 nm to 500 nm. After oxidation, the bottom electrode layer is deposited using a PVD process, typically sputtering. The piezoelectric material dictates the choice of the bottom electrode material. Our study uses lead zirconate titanate (PZT), which works best with a platinum bottom electrode. The quality and crystal orientation of the underlying bottom electrode have a bearing on the quality of the deposited piezoelectric film. A titanium (Ti) or a titanium dioxide ($TiO2$) film with a thickness of a 20 nm-40 nm is used as the adhesion enhancement layer to ensure that the platinum film firmly sticks to the substrate below.

We used sol-gel deposited PZT films that were prepared at our Centre, and also films that we outsourced from Quintess Co. Ltd., S. Korea. Most of the results presented here are from the film that we obtained from Quintess.

Figure 2 shows a scanning electron micrograph of the cross-section of a wafer after the deposition of the platinum and PZT films. The top layer is the PZT which has a thickness of about 840 nm in this case. The crystal orientation of the films was characterized using an X-Ray Diffractometer from Rigaku Corporation. Figure 3 shows the results of the $\theta/2\theta$ scan of the deposited PZT film. The peaks corresponding to PZT planes are indicated in brackets, except for the prominent Pt (111) peak and the Si peak. It can be seen that the PZT film is primarily oriented along the (111) plane.

The SOI wafer with the bottom electrode and piezoelectric film serves as the substrate for further fabrication. The first lithography step involves the patterning and deposition of the top electrodes. In our case, this is done using the lift-off process. After the deposition of the top electrode, areas of the piezoelectric film are selectively etched to create pads to access the bottom electrode. This completes the processing on the top side of the SOI wafer. All designs discussed here have used a continuous blanket bottom electrode, and hence all PMUTs on a die have a common bottom electrode.

The next steps consist in the back-side etching of the handle silicon layer to release the PMUT diaphragms using a highly anisotropic dry etching process like DRIE (deep reactive ion etching). DRIE has the advantage of producing highly rectangular walls with high aspect ratios, minimizing the undercut. This is important to ensure that the diaphragm dimensions are maintained during the etching. The DRIE etches the handle silicon layer till the buried silicon oxide is exposed, which acts as the etch stop. This ensures that even in the case of uneven etching over the wafer area, the thickness of the diaphragms does not vary since the DRIE always lands on the buried oxide. After DRIE, the buried oxide layer is removed using RIE to reveal the bottom side of the device layer silicon, completing the microfabrication and micromachining of the PMUT devices. We also include

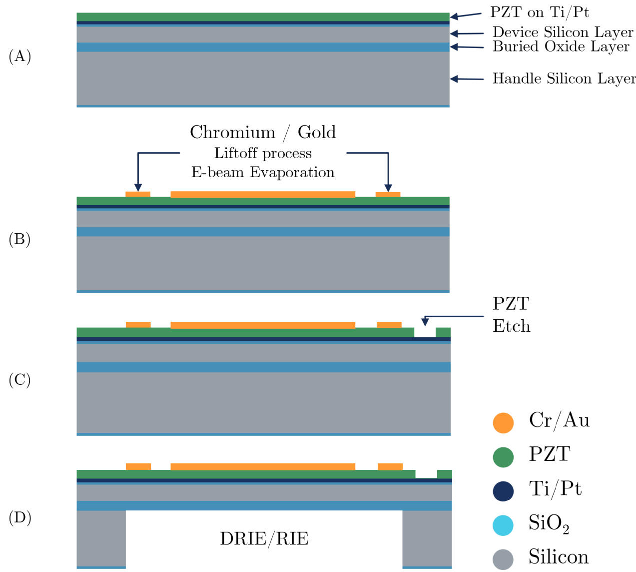


**FIGURE 4. PMUT fabrication process flow using PZT-coated SOI wafer.**

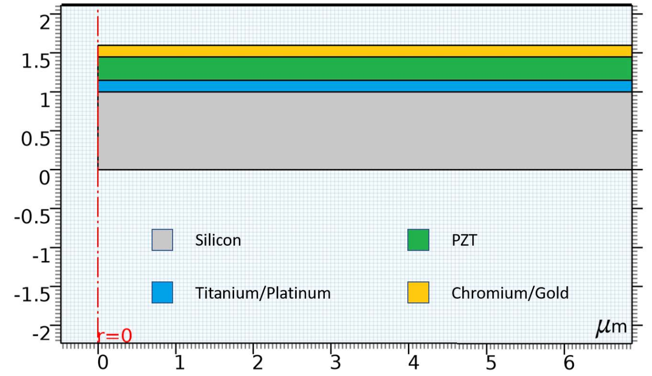


**FIGURE 5. Thin-film stack used in the COMSOL model showing the material models used for different layers.**

the dicing lines in the DRIE mask to assist with the separation of individual dies and avoid a saw-based dicing step.

The thickness of the structural layer of the diaphragm is determined by the thickness of the device layer silicon. SOI wafers are available in a range of stack configurations, and it is essential to decide this thickness since it cannot be easily changed post-fabrication. The different geometric parameters of a PMUT, their origin and the flexibility in their values are summarized below.

- **Structural layer thickness** - Determined by the device layer thickness of the SOI wafer. Difficult to change after wafer procurement.
- **Electrode and PZT layer thickness** - Determined during deposition steps. Can be varied in a limited range, but usually fixed by an optimized recipe.
- **Diaphragm diameter** - Determined by lithography mask. Devices with a range of diameters can be fabricated on the same wafer.

## IV. NATURAL FREQUENCY OF A PMUT

In this study, our aim is to design PMUTs with resonance frequencies suitable for the transmission of data-over-sound in the near-ultrasound band. To this end, we first look at the analytical expression for the natural frequency of a PMUT. The diaphragm of a PMUT can be treated as a clamped circular plate with pre-tension. The natural frequency of the first eigenmode or the *breathing mode* of such a circular plate can be expressed as:

$$\omega_{00} = \alpha_{00}\beta_{00}\sqrt{\frac{D_e}{\rho_h a^4}} = \sqrt{\frac{\alpha_{00}^2 D_e}{\rho_h a^4}(\alpha_{00}^2 + \kappa^2)} \quad . \tag{1}$$

The non-dimensional parameter pair $\alpha_{mn}$ and $\beta_{mn}$ depend on the natural modes of vibration of the plate, where the subscripts $m$ and $n$ indicate the number of nodal circles and nodal diameters respectively. For the first eigenmode, $m = n = 0$. $D_e$ is the flexural rigidity of the diaphragm, $\rho_h$ is the density of the diaphragm material, and $a$ is the radius of the diaphragm. The quantity $\kappa^2$ is the non-dimensional tension to flexural rigidity ratio and determines whether the diaphragm behaves as a plate or a membrane. A detailed derivation and treatment of this formula has been presented in [10] and [11].

We use this equation to analyze the variation of $\kappa^2$ and the frequency parameters by plugging in typical values of residual stress, device layer thickness and diameters to study the fundamental frequency ($\omega_{00}$) in different regimes. The calculation results are presented at the end of the next section, along with the results of the finite element simulation.

## V. SIMULATION

Finite element simulations of the PMUTs were carried out in COMSOL 5.4 to verify the analytical formulation for the natural frequency, especially in extreme cases, and to arrive at optimum design parameters. The diaphragm of our PMUT consists of a stack of thin films comprising the device layer silicon, the platinum bottom electrode, the PZT layer and the gold top electrode. A 2D axisymmetric model of the diaphragm was created and meshed using mapped quad elements. The handle layer was not modeled, and the diaphragm was clamped at the circumference. A zoomed in view of the FEM model is shown in Figure 5.

A parametric eigenfrequency study was carried out by changing the dimensions of the diaphragm and by varying the residual tension $\sigma_r$, structural layer thickness $t_{Si}$ and diaphragm diameter $d_{Si}$. The thickness of both the bottom Pt and the top Au electrodes was set to 150 nm. The thickness of the structural layer and the stress in the PZT layer were defined as variable parameters. The details of the parameters are listed in Table 2. An initial static study was performed to calculate the diaphragm's initial deformation (or linearization point) due to the residual stress, before performing the eigenfrequency analysis on it.

Linear, elastic, isotropic models were used for each material layer. The residual stress $\sigma_r$ in the PZT layer was

**TABLE 2. Range and step sizes of PMUT design parameters for sweep of eigenfrequency study.**

| Parameter | Value | Step Size |
|---|---|---|
| Residual Stress, $\sigma_r$ (MPa) | 0 - 1500 | 100 |
| Device layer thickness, $t_{Si}$ ($\mu$m) | 1 - 30 | 1 |
| Diameter, $d_{Si}$ (mm) | 1 - 5 | 0.5 |
| PZT thickness, $t_{PZT}$ (nm) | 900 | - |
| Electrode thickness (nm) | 150 | - |

**TABLE 3. Material properties used in the finite element simulation of the PMUT.**

| Parameter | Si | Pt | PZT | Au |
|---|---|---|---|---|
| Density (kg/m$^3$) | 2329 | 21450 | 7500 | 19300 |
| Young's modulus (GPa) | 170 | 168 | 110 | 70 |
| Poisson's Ratio | 0.28 | 0.38 | 0.39 | 0.44 |

t_si=10, r_si=2250, pzt_stress=300, t_pzt=900 Eigenfrequency=17401 Hz

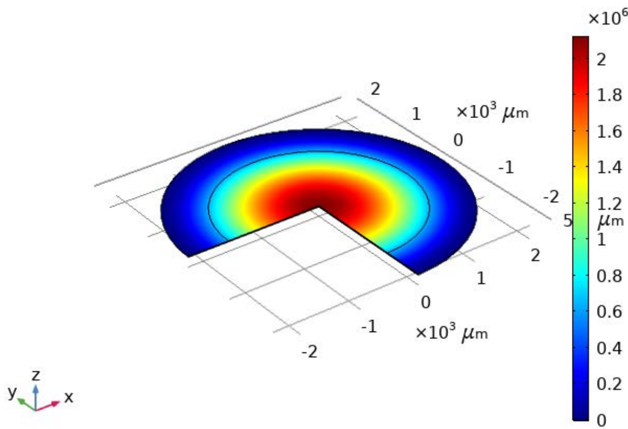


**FIGURE 6. Simulated pseudo-color map of the modeshape for the first Eigen frequency of a membrane type PMUT.**

modelled as *Initial Stress* in COMSOL, in the X and Y directions (in-plane stress). The material properties used are listed in Table 3.

Figure 6 shows the mode shape for the first eigenmode, or the *breathing mode*, of a circular diaphragm. The figure is presented as an expanded three-fourths view of the axisymmetric solution. The frequency of this first eigenmode was considered for the analysis and the preparation of the design maps.

### A. DESIGN MAPS

The natural frequency of a PMUT depends on various material and geometric factors that can be controlled to different degrees as described in Section III. Among the geometric factors, it is much easier to change the diameter of a PMUT by changing the design of the lithography masks, but it is relatively difficult to change the thickness of the device layer of the SOI wafer. Wafers are often bought in large batches, where each wafer has the same specifications. SOI wafers are available in a wide variety of stack configurations, with

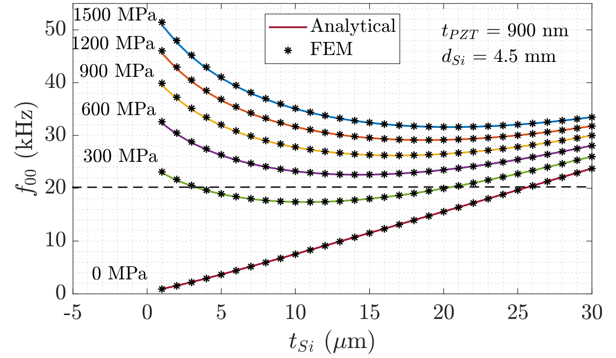


**FIGURE 7. Variation of natural frequency with thickness of the structural silicon layer, for different values of residual stress. As a reference, the dashed line at 20 kHz, indicates the upper threshold of human hearing.**

device layer thickness varying between tens of nanometres to hundreds of micrometres. We investigated the variation of the natural frequency of a PMUT with device layer thickness to ascertain the best value closest to the available SOI device layer thicknesses to get the lowest natural frequency for the values of stress in the films.

We measured the magnitude of the residual stresses using a kSA MOS UltraScan tool from k-Space Associates. The tool uses a two-dimensional laser array to map the curvature and bow in a wafer, and compute the residual stress. The values of residual tensile stress were found to be around 300 MPa, and did not vary significantly from one run to another.

Figure 7 depicts the variation in the frequency of the fundamental mode $f_{00}$ (in kHz, using $\omega_{00}/2000\pi$) with diaphragm thickness $t_{Si}$, within a range of residual stress in the piezoelectric layer, for a fixed PZT thickness $t_{PZT}$ and diaphragm diameter $d_{Si} = 4.5$ mm.

There is an excellent agreement between the analytical formula shown in Eq. 1 and the FEM simulation. When there is no stress acting on the piezoelectric layer, $D_e$ dominates and therefore the variation between $f_{00}$ and $t_{Si}$ becomes linear. Thus, the diaphragm's vibrational response purely follows that of a plate. However, this trend deviates in the presence of any tensile $\sigma_r$ in the PZT layer, where the relation between $f_{00}$ and $t_{Si}$ begins to bow upwards for thin diaphragms. This can be attributed to the diaphragm behaving as a tensioned membrane wherein the stiffening effect offered by the $T_e$ begins dominating $D_e$ of the structural layer. From the graph, the lowest frequency can be found between a thickness of 10 µm to 20 µm. We used PZT-coated SOI wafers with a 10 µm device layer thickness to fabricate devices in a range of diameters to verify the simulation results.

## VI. EXPERIMENTS

### A. FABRICATION

To verify the results of simulations, we designed a mask with PMUT diameters in the range of 3 mm to 5 mm with increments of 0.5 mm or 500 µm. Figure 8 shows the layout of a single D4500 PMUT with 3 layers — the top electrode

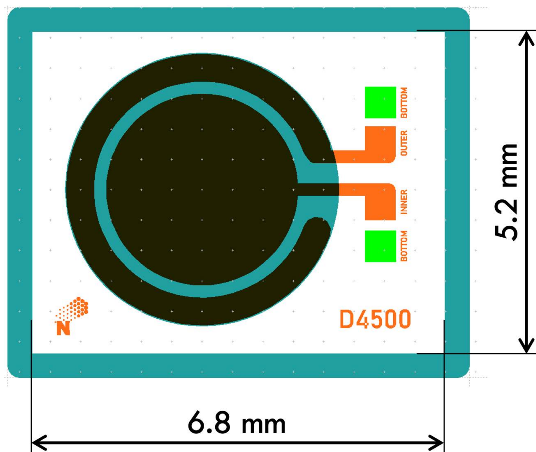


**FIGURE 8. Detailed mask of a single D4500 PMUT showing the inner and outer electrodes.**

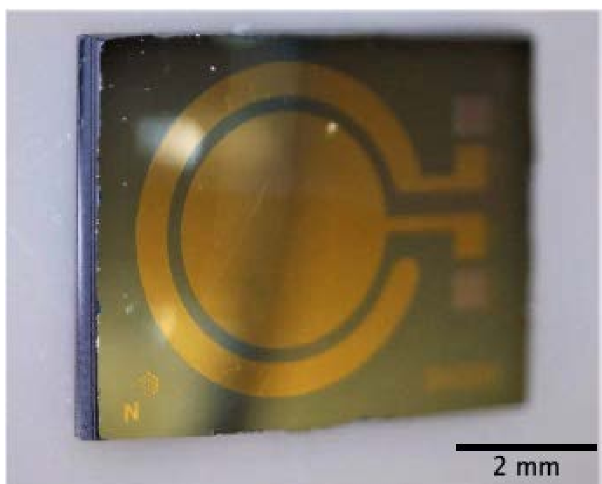


**FIGURE 9. A separated die of a single D4500 transducer after fabrication, but before wire-bonding.**

in orange, PZT etch in green, and the bottom DRIE etch in teal. Figure 9 shows a photograph of a single D4500 PMUT after die-separation.

### B. POLING AND PACKAGING

The transducers were poled by heating the dies to 100 °C and then gradually applying a DC voltage of up to 10 V between the top and the bottom electrodes. The applied electric field was held for about 20 minutes, after which the devices were allowed to cool down with a small voltage of 2 V still applied. The DC flowing through the devices was limited using a Source Measure Unit (SMU) to 100 µA to avoid damage to the devices due to any formation of transient leaky current paths. After poling, the devices were epoxy-bonded and wire-bonded to custom-designed PCBs.

### C. MECHANICAL CHARACTERIZATION

The electromechanical response of each device was measured using a Polytec Micro System Analyser MSA500 Laser

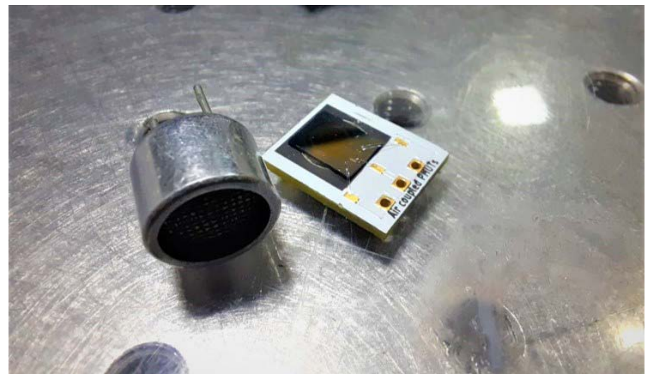

**FIGURE 10. A D4500 PMUT epoxy- and wire-bonded to a PCB next to a 10 mm 40 kHz ultrasound transducer.**

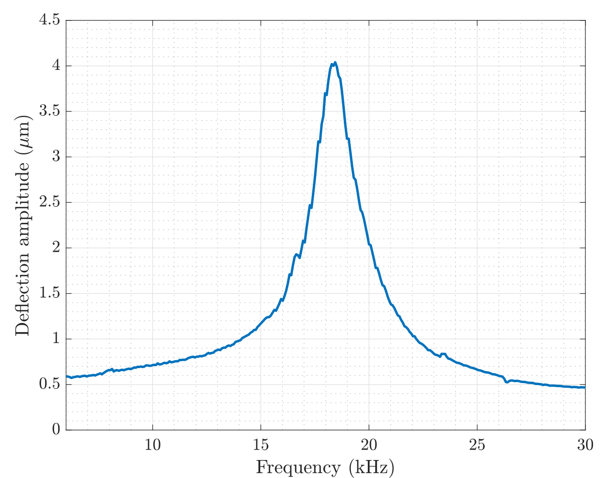


**FIGURE 11. Frequency response of the centre deflection of a D4500 PMUT measured using laser Doppler vibrometry at 10 V excitation.**

Doppler Vibrometer (LDV) at the Micro and Nano Characterization Facility (MNCF) at CeNSE. Frequency sweep studies were performed using chirp and sinusoidal signals applied at the device terminals. Figure 11 shows the frequency response of a D4500 PMUT measured using an LDV.

Figure 12 shows the variation of natural frequency with diameter of the diaphragm for different values of residual stress. As a reference, the dashed line at of 20 kHz indicates the upper threshold of human hearing. The black markers indicate the frequency values measured using the LDV and the error bars indicate the spread of the natural frequency measured for 5 different devices. The measured first mode frequencies closely follow the trend for a simulated stress of 300 MPa.

The minor deviations between the measured and simulated values can be attributed to differences in the actual versus simulated boundary conditions of the PMUT, where the handle layer was not modelled. The simulation also ignores the presence of residual stresses in all thin-film layers except PZT that can occur during the fabrication process.

Small variations within experimental results for devices of the same diameter can be attributed to variability in the

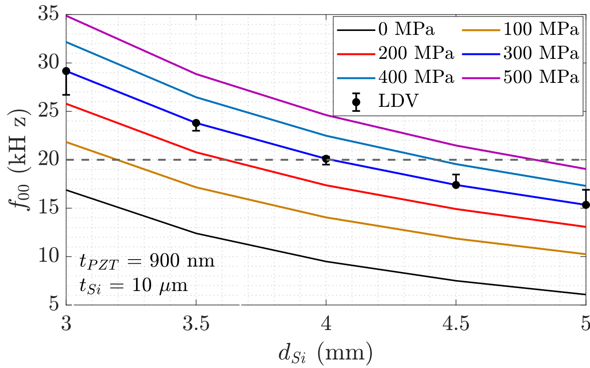


FIGURE 12. Variation of natural frequency with diameter of the diaphragm, for different values of residual stress.

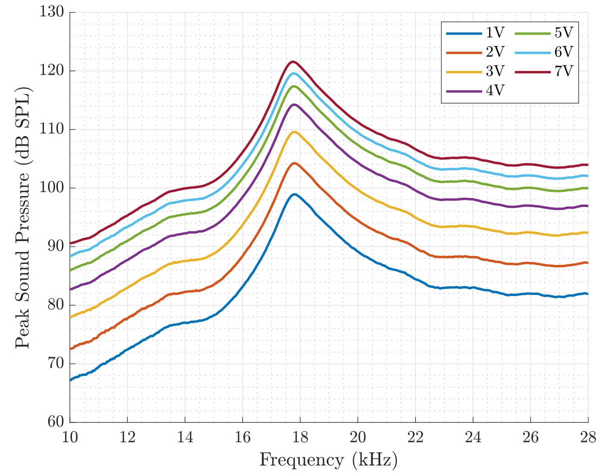


FIGURE 13. Acoustic frequency response plots for a D4500 PMUT with different input signal voltage levels.

fabrication processes. The DRIE process used here allows us to control the lateral dimension of the cavity and the diaphragm accurately. However, there can be small variations in the thickness of the diaphragm in different regions of the wafer due to loading effects and non-uniformity of the RIE plasma leading to undercut in some diaphragms. Figure 7 suggests that the frequency of the first mode is not very sensitive to the thickness near the relatively flat region in the middle of the graphs.

### D. ACOUSTIC CHARACTERIZATION

The device's radiated sound pressure level and sound field were recorded using a customized measurement setup [22]. A 3D printer was reconfigured to behave as a computer-controlled 3-axis motion system for positioning a reference microphone (GRAS 46DP-1). The microphone was polarized with a suitable power supply (Brüel & Kjær Type-2829) at 200 V. The transducer was placed on the bed of the 3D printer and driven using a lock-in amplifier (Zurich Instruments MFLI). This allowed for convenient on-axis sound pressure measurements as well as mapping the radiated sound field of the given source by sampling the pressure in a grid-like pattern in front of it.

Figure 13 shows the sound-pressure vs. frequency response curves obtained from the transducer at a distance of 1 cm from the surface of the die for different excitation voltage levels. The sound pressures exceed 120 dB at this distance. The transducer shows a linear response with voltage and shows no non-linear hardening or softening trends in the frequency response at up 7 V. The −6 dB bandwidth of the transducers is observed to be 2 kHz and the transducers have a quality factor of around 9.

We automated the motion of the microphone and the measurement setup using LabVIEW to physically map the sound field of a given source by sampling the pressure in a grid-like pattern over it. Figure 14 shows a schematic of the scanner used for time-domain measurements. The function generator and the data acquisition system were replaced with a lock-in amplifier (Zurich Instruments MFLI) to perform frequency

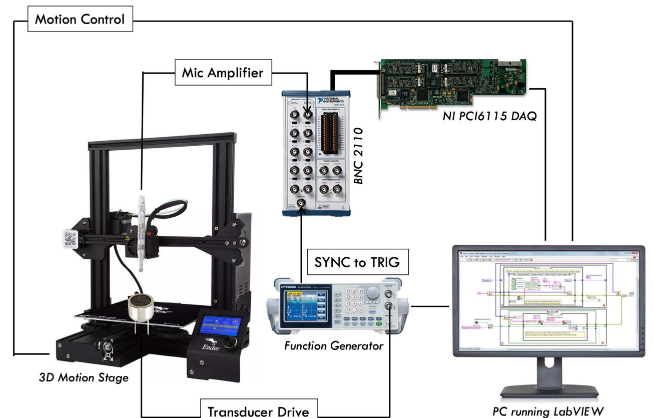


FIGURE 14. Schematic of the acoustic field scanning system for time-domain and frequency-domain measurements.

sweep measurements to obtain the frequency response of transducers.

Figure 15 shows a 5 cm x 5 cm sound field map of a D4500 PMUT measured in an axial plane when excited at its resonance with a 1 V sinusoidal signal. The colour bar shows the sound pressure levels in dB SPL, and the axes indicate the distance in millimetres. The transducer was placed at the bottom center of the plot, at X = 25 mm. It can be observed that the transducer has a prominent central lobe and is not completely omnidirectional.

### E. ELECTRICAL CHARACTERIZATION

The power consumption of the device was measured by recording the RMS voltage across and the current through the transducer using two Fluke 287 TrueRMS multimeters. The PMUT was driven with single-tone sinusoidal signals using a function generator and an amplifier circuit based on an AD8606 op-amp from Analog Devices. The amplifier has a typical gain-bandwidth product of 10 MHz and was used in a non-inverting configuration with a nominal gain of 2.

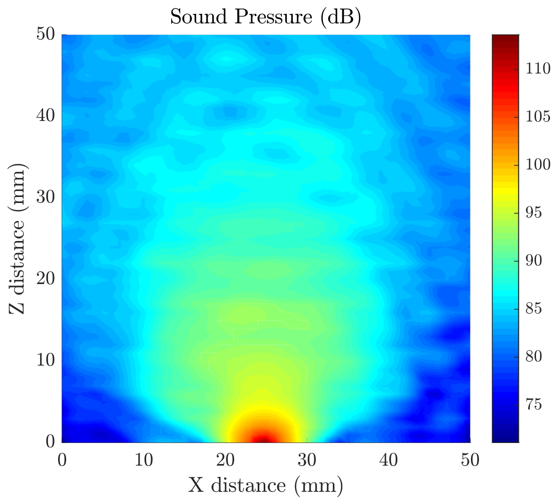


**FIGURE 15. Sound field map of a D4500 PMUT with a 4.5mm diameter. The colour bar represents the sound pressure level in dB SPL.**

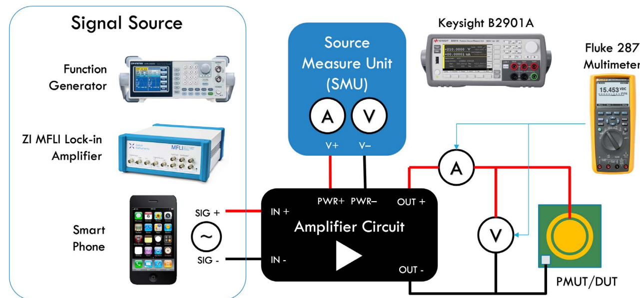


**FIGURE 16. Schematic of the circuit used for electrical power measurements showing the signal source, amplifier circuit, the SMU to power the amplifier circuit, the PMUT/DUT and the two multimeters that were used to measure the voltage across and current through the transducer.**

Figure 16 shows the schematic of the setup used for electrical power measurement. The power draw of the PMUT was measured using the multimeters, and the power draw of the amplifier was recorded using the Keysight B2901A Source Measure Unit (SMU). Figure 17 shows the power draw of the PMUT. The power consumption of the PMUT is observed to rise with increasing frequency. The PMUT works on the principle of the inverse piezoelectric effect, and therefore, it behaves as a capacitive device. The net electrical impedance offered by a capacitive device decreases with increasing frequency as $(j\omega C)^{-1}$, with $C$ being the PMUT's capacitance. This causes the current draw to rise with frequency and thereby increases the power draw. The power consumption of the PMUT was found to be around 18 mW, which is nearly an order of magnitude lower than a conventional electrodynamic speaker at 170 mW for the same output sound pressure. The electrodynamic speaker used here for comparative power measurement was a commercial 2030 micro-speaker with dimensions of 20 mm × 30 mm and a nominal impedance of 8 Ω.

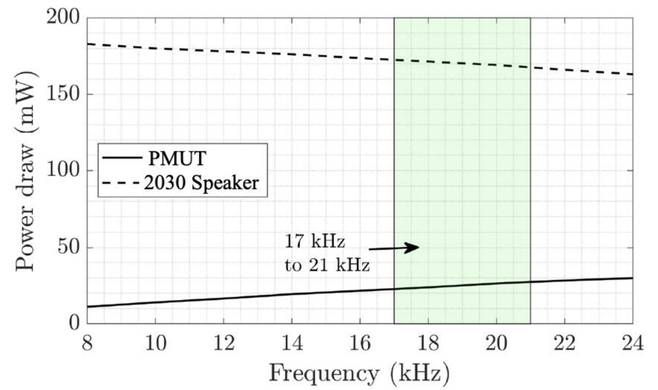


**FIGURE 17. Power draw comparison between PMUT and a 2030 microspeaker, both driven at 1.414 $V_{rms}$.**

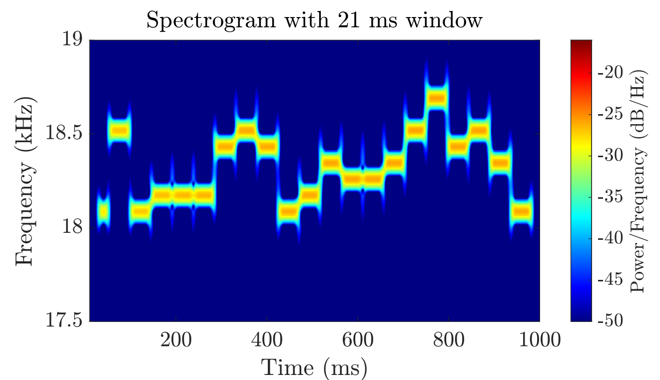


**FIGURE 18. Spectrogram of raw test signal, for the test sequence "1234567890" encoded in FSK.**

## VII. DoS PERFORMANCE

The capabilities of the PMUT as a viable transmitter for DoS communication are discussed in this section. We measure the peak power draw and the corresponding distance for successful transmission and reception of a test signal. For our experiment, we used a proprietary frequency-shift-keying (FSK) encoder in the form of a smartphone app from ToneTag (Naffa Innovations Pvt. Ltd.). A string of digital data was transmitted as a sequence of near-ultrasound pulses within the range of 18 kHz to 19 kHz. The recording and processing of the sound signals was handled by the smartphone app. The sampling of all signals was performed at 44.1 kHz. A spectrogram generated from a raw .wav file of the test signal is shown in Fig. 18.

Two smartphones, A and B, were used for transmitting and receiving signals respectively (Figure 19). Phone A's task was to generate the FSK encoded waveform and feed it as the input to the PMUT, the other Phone B's task was to decode the sequence of pulses transmitted by the PMUT. An amplifier similar to the one shown in Figure 16 was used to amplify the signals and drive the PMUT.

### A. PEAK POWER CONSUMPTION

Figure 20 illustrates the instantaneous power consumption during the transmission of the test signal, as measured with a

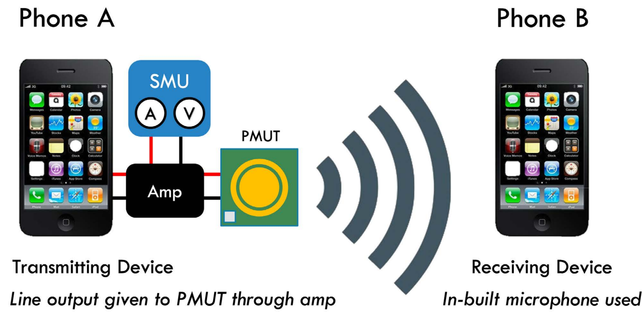


**FIGURE 19. Schematic of the setup with two smartphones used for data transmission experiments.**

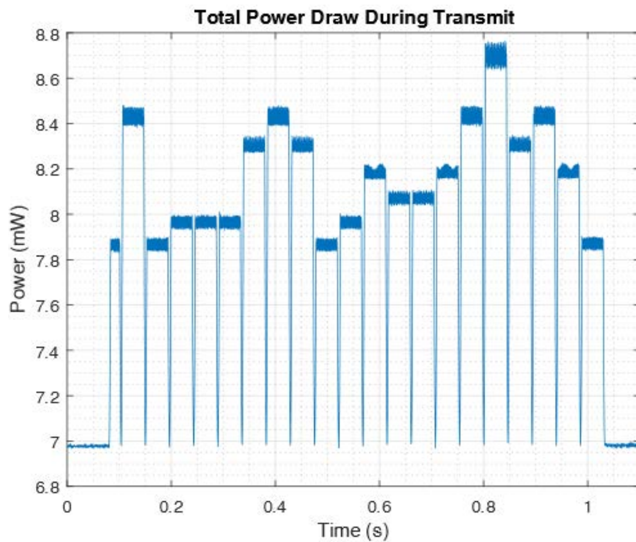


**FIGURE 20. Power consumption during transmit, for the sequence "1234567890."**

source-measurement unit (SMU) (Figs. 16 and 19) by measuring the total current draw of the amplifier used to drive the PMUT.

The total power draw is shown to vary between 6.98 mW and 8.76 mW during transmission of the signal. Out of this, the amplifier consumed 6.98 mW due to its quiescent current draw of 2.32 mA at 3 V, while the remaining power draw of 1.88 mW was that due to transmission of the signal by the PMUT.

Communication was considered successful when the received pulses were decoded successfully. For our experiment, the volume of smartphone A was increased in steps of 10% of its maximum while smartphone B was moved away from the PMUT until the point where DoS communication failed. The distance between the PMUT and B was measured using a laser range finder.

Figure 21 presents the variation of reception range with the peak power draw of the PMUT during transmission of the test sequence. The power draw values are proportional to the output volume used in smartphone A. It can be observed that the PMUT is capable of establishing communication at a distance of up to 6 m while consuming less than 10 mW of peak power. The relationship between reception range and peak power draw is not linear as the PMUT starts to consume as much as 76 mW for a reception range of 12 m.

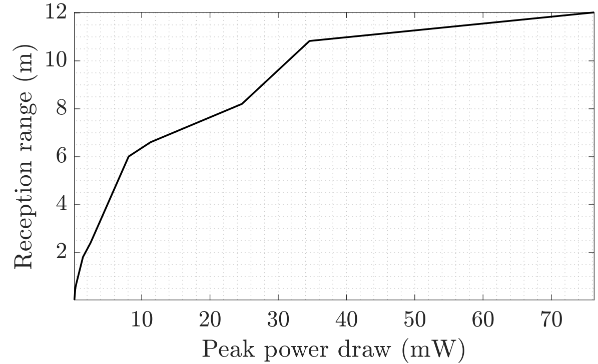


**FIGURE 21. DoS communication range, for the sequence "1234567890."**

## VIII. CONCLUSION

A low frequency PMUT operating at the upper bounds of human hearing was successfully fabricated and tested as a viable transmitter for DoS applications. Using analytical modelling and simulation, we arrived at the optimum thickness of the passive structural layer to minimize the footprint of the transducers. We observed that the range of thickness between 10 µm and 20 µm gives the lowest value of resonant frequencies in the desired range for a wide range of fabrication induced residual tensile stresses. Using fabricated PMUTs, we validated the simulations and found that the D4000 and the D4500 PMUTs with diameters of 4 and 4.5 mm and mechanical resonance frequencies of 19.5 kHz and 18 kHz, respectively, are ideal candidates for transmitting data-over-sound. The transducers were found to have power consumption values that were at least an order of magnitude lower than the conventional microspeakers in the frequency range of interest with similar sound pressure output.

## ACKNOWLEDGMENT

An earlier version of this paper was presented at the 2020 IEEE International Ultrasonics Symposium (IUS) and was published in its proceedings [DOI: 10.1109/IUS46767.2020.9251747]. The transducers were fabricated at the National Nano Fabrication Centre (NNFC) and characterized at the Micro and Nano Characterization Facility (MNCF). The authors thank the Ministry of Electronics and Information Technology (MeitY); and the Department of Science and Technology (DST), Government of India, for their support of NNFC and MNCF. The authors would also like to thank Dr. Antony Jeyaseelan for his help with the deposition and characterization of the PZT thin films.

## REFERENCES

[1] P. Getreuer, C. Gnegy, R. F. Lyon, and R. A. Saurous, "Ultrasonic communication using consumer hardware," *IEEE Trans. Multimedia*, vol. 20, no. 6, pp. 1277–1290, Jun. 2018.

[2] H. Kazari, M. Kabir, A. Mostavi, and D. Ozevin, "Multi-frequency piezoelectric micromachined ultrasonic transducers," *IEEE Sensors J.*, vol. 19, no. 23, pp. 11090–11099, Dec. 2019.

[3] B. Chen, F. Chu, X. Liu, Y. Li, J. Rong, and H. Jiang, "AlN-based piezoelectric micromachined ultrasonic transducer for photoacoustic imaging," *Appl. Phys. Lett.*, vol. 103, no. 3, Jul. 2013, Art. no. 031118.

[4] A. Dangi *et al.*, "A modular approach to neonatal whole-brain photoacoustic imaging," in *Proc. SPIE*, vol. 11240, A. A. Oraevsky and L. V. Wang, Eds. Feb. 2020, pp. 317–325.

[5] H.-Y. Tang *et al.*, "3-D ultrasonic fingerprint sensor-on-a-chip," *IEEE J. Solid-State Circuits*, vol. 51, no. 11, pp. 2522–2533, Nov. 2016.

[6] O. Rozen *et al.*, "Monolithic MEMS-CMOS ultrasonic rangefinder based on dual-electrode PMUTs," in *Proc. IEEE 29th MEMS*, Jan. 2016, pp. 115–118.

[7] K. Roy *et al.*, "Fluid density sensing using piezoelectric micromachined ultrasound transducers," *IEEE Sensors J.*, vol. 20, no. 13, pp. 6802–6809, Jul. 2020.

[8] H. Gupta, B. Nayak, K. Roy, A. Ashok, A. A. Jeyaseelan, and R. Pratap, "Development of micromachined piezoelectric near-ultrasound transducers for data-over-sound," in *Proc. IEEE Int. Ultrason. Symp. (IUS)*, Sep. 2020, pp. 1–4.

[9] F. Sammoura, K. Smyth, S. Bathurst, and S.-G. Kim, "An analytical analysis of the sensitivity of circular piezoelectric micromachined ultrasonic transducers to residual stress," in *Proc. IEEE Int. Ultrason. Symp.*, Oct. 2012, pp. 580–583.

[10] A. Dangi and R. Pratap, "System level modeling and design maps of PMUTs with residual stresses," *Sens. Actuators A, Phys.*, vol. 262, pp. 18–28, Aug. 2017.

[11] M. Olfatnia, T. Xu, L. S. Ong, J. M. Miao, and Z. H. Wang, "Investigation of residual stress and its effects on the vibrational characteristics of piezoelectric-based multilayered microdiaphragms," *J. Micromech. Microeng.*, vol. 20, no. 1, Jan. 2010, Art. no. 015007.

[12] S. Lee, T. Tanaka, K. Inoue, J.-M. Kim, Y.-E. Shin, and M. Okuyama, "Stress influences on the ultrasonic transducers," *Sens. Actuators A, Phys.*, vol. 119, no. 2, pp. 405–411, Apr. 2005.

[13] P. Simeoni, Z. Schaffer, and G. Piazza, "A 100 nm thick, 32 kHz X-cut lithium niobate piezoelectric nanoscale ultrasound transducer for airborne ultrasound communication," *J. Microelectromech. Syst.*, vol. 30, no. 3, pp. 337–339, Jun. 2021.

[14] G.-L. Luo, Y. Kusano, M. N. Roberto, and D. A. Horsley, "High-pressure output 40 kHz air-coupled piezoelectric micromachined ultrasonic transducers," in *Proc. IEEE 32nd Int. Conf. Micro Electro Mech. Syst. (MEMS)*, Jan. 2019, pp. 787–790.

[15] P. Simeoni and G. Piazza, "Enhanced airborne ultrasound WuRx using aluminum nitride 4-beam pNUTs arrays," *J. Microelectromech. Syst.*, vol. 31, no. 1, pp. 150–157, Feb. 2022.

[16] A. Dangi, A. Hulge, A. Somasundaran, R. S. Valsalam, and R. Pratap, "Complete development of a single cell PMUT transducer: Design, fabrication, characterization, and integration," *J. Inst. Smart Struct. Syst.*, vol. 4, no. 41, pp. 61–69, 2015.

[17] Z. Wang, W. Zhu, J. Miao, H. Zhu, C. Chao, and O. K. Tan, "Micromachined thick film piezoelectric ultrasonic transducer array," *Sens. Actuators A, Phys.*, vols. 130–131, pp. 485–490, Aug. 2006.

[18] K. H. Been, Y. U. B. Je, H. S. Lee, and W. K. Moon, "A parametric array PMUT loudspeaker with high efficiency and wide flat bandwidth," in *Proc. 18th Int. Conf. Solid-State Sens., Actuat. Microsyst.*, Jun. 2015, pp. 2097–2100.

[19] G. Massimino, L. D'Alessandro, F. Procopio, R. Ardito, M. Ferrera, and A. Corigliano, "Air-coupled PMUT at 100 kHz with PZT active layer and residual stresses: Multiphysics model and experimental validation," in *Proc. 18th Int. Conf. Thermal, Mech. Multi-Phys. Simul. Exp. Microelectron. Microsyst. (EuroSimE)*, Apr. 2017, pp. 6–9.

[20] Z. Zhou, S. Yoshida, and S. Tanaka, "Epitaxial PMnN-PZT/Si MEMS ultrasonic rangefinder with 2 M range at 1 V drive," *Sens. Actuators A, Phys.*, vol. 266, pp. 352–360, Oct. 2017.

[21] R. J. Przybyla *et al.*, "In-air rangefinding with an ALN piezoelectric micromachined ultrasound transducer," *IEEE Sensors J.*, vol. 11, no. 11, pp. 2690–2697, Nov. 2011.

[22] B. Nayak, H. Gupta, K. Roy, A. Ashok, V. Shastri, and R. Pratap, "An experimental study of the acoustic field of a single-cell piezoelectric micromachined ultrasound transducer (PMUT)," 2021, *arXiv:2108.04660*.

**HARSHVARDHAN GUPTA** (Student Member, IEEE) received the B.Tech. degree in mechanical engineering from the National Institute of Technology Karnataka Surathkal, Surathkal, India, in 2012, and the M.S. degree in mechatronics from FH Aachen, Germany, in 2017. He is currently pursuing the Ph.D. degree with the Centre for Nanoscience and Engineering (CeNSE), Indian Institute of Science (IISc), Bengaluru, India. He is a Research Associate with the ECE Department, Carnegie Mellon University, Pittsburgh, PA, USA. His research interests include MEMS/MOEMS, ultrasound, acoustics, and vibrations.

**BIBHAS NAYAK** received the B.Tech. degree in control systems from the Manipal Institute of Technology in 2016 and the M.Sc. degree in engineering acoustics from the Technical University of Denmark in 2019. He is the Lead Audio Engineer with Reliance Jio Tesseract. He previously worked with the MEMS Laboratory, Centre for Nanoscience and Engineering (CeNSE), Indian Institute of Science (IISc), Bengaluru, India, undertaking research on piezoelectric transducers.

**ANUJ ASHOK** (Student Member, IEEE) received the B.E. degree in mechanical engineering from the Srinivas Institute of Technology, Mangaluru, India, in 2016, and the M.Tech. degree in nanotechnology from the National Institute of Technology Karnataka Surathkal, Surathkal, India, in 2018. He is currently pursuing the Ph.D. degree with the Elmore Family School of Electrical and Computer Engineering, Purdue University, USA. He worked as a Project Associate with the MEMS Laboratory, Centre for Nanoscience and Engineering, Indian Institute of Science, Bengaluru, from 2018 to 2021. His research interests include MEMS, VLSI fabrication, ultrasound, and diamond color centers.

**RUDRA PRATAP** (Senior Member, IEEE) received the B.Tech. degree from the Indian Institute of Technology Kharagpur, Kharagpur, India, in 1985, the master's degree in mechanics from The University of Arizona, Tucson, in 1987, and the Ph.D. degree in theoretical and applied mechanics from Cornell University, Cornell, NY, USA, in 1993. He is currently a Professor with the Centre for Nanoscience and Engineering (CeNSE), Indian Institute of Science (IISc), Bengaluru, India; and the Founding Vice Chancellor with Plaksha University, Sahibzada Ajit Singh Nagar, India. His research interests include MEMS design, computational mechanics, nonlinear dynamics, structural vibration, and vibroacoustics.